Preprints.org

Article

Not peer-reviewed version

Mapping Leaf Area Index at Various Rice Growth Stages in Southern India Using Airborne Hyperspectral Remote Sensing

Mathyam Prabhakar *, Kodigal A. Gopinath, Ravi Kumar Nakka, Merugu Thirupathi, Uppu Sai Sravan, Golla Srasvan Kumar, Gutti Samba Siva, Pebbeti Chandana, Vinod Kumar Singh

Posted Date: 26 December 2023

doi: 10.20944/preprints202312.2021.v1

Keywords: hyperspectral remote sensing; vegetation indices; canopy reflectance; leaf area

Preprints.org is a free multidiscipline platform providing preprint service that is dedicated to making early versions of research outputs permanently available and citable. Preprints posted at Preprints.org appear in Web of Science, Crossref, Google Scholar, Scilit, Europe PMC.

Copyright: This is an open access article distributed under the Creative Commons Attribution License which permits unrestricted use, distribution, and reproduction in any medium, provided the original work is properly cited.

Preprints (www.preprints.org) | NOT PEER-REVIEWED | Posted: 26 December 2023 doi:10.20944/preprints202312.2021.v1

Disclaimer/Publisher's Note: The statements, opinions, and data contained in all publications are solely those of the individual author(s) and contributor(s) and not of MDPI and/or the editor(s). MDPI and/or the editor(s) disclaim responsibility for any injury to people or property resulting from any ideas, methods, instructions, or products referred to in the content.

Article

Mapping Leaf Area Index at Various Rice Growth Stages in Southern India Using Airborne Hyperspectral Remote Sensing

Mathyam Prabhakar *, Kodigal A Gopinath, Nakka Ravi Kumar, Merugu Thirupathi, Uppu Sai Sravan, Golla Srasvan Kumar, Gutti Samba Siva, Pebbeti Chandana and VK Singh

ICAR-Central Research Institute for Dryland Agriculture, Santoshnagar, Hyderabad - 500059, India

* Correspondence: prab249@gmail.com

Abstract: Globally, rice is one of the most important staple food crops. The most significant metric for evaluating the rice growth and productivity is the Leaf Area Index (LAI), which can be effectively monitored using remote sensing data. Hyperspectral remote sensing provides contiguous bands at narrow wavelengths for mapping LAI at various rice phenological stages and it is functionally related to canopy spectral reflectance. Hyperspectral signatures for different phases of rice crop growth was recorded using Airborne Visible Near-Infrared Imaging Spectrometer - Next Generation (AVIRIS-NG) along with corresponding ground based observations. Ground based hyperspectral canopy spectral reflectance measurements was recorded with FieldSpec 3 Hi-Res spectroradiometer (ASD Inc., USA; spectral range: 350-2500 nm) and LAI data from 132 farmer's fields in Southern India. Among 29 hyperspectral vegetation indices tested, eight were found promising for mapping rice LAI at various phenological stages. Among all the growth stages, elongation stage was the most accurately estimated using vegetation indices that exhibited significant correlation with the airborne hyperspectral reflectance. The validation of hyperspectral vegetation indices revealed that the best fit model for estimating rice LAI was mND_{705} (red-edge, blue and NIR bands) at seedling and elongation, SAVI (red and NIR bands) at tillering and WDRVI (red and NIR bands) at booting stage.

Keywords: hyperspectral remote sensing; vegetation indices; canopy reflectance; leaf area

1. Introduction

Global rice production was 513.68 mt, of which, India contributes to 132 mt after China, and plays an important role in the global rice economy [1]. India ranks second in consumption which attributes to the adequate supply of rice leading to food security. Remote sensing technology has gained attention as it provides rapid and macro-scale observations using spectral data of the crop canopy to ameliorate the crop growth parameter estimation [2–4]. The reflectance curve in the red and blue region displays a valley when the plant canopy is healthy as it significantly absorbs blue and red light and reflect green light [5]. Thus, higher reflectance in the near infrared region (NIR) was closely associated with internal cell structure, biomass, vegetation cover, leaf water content, and LAI, whereas red-edge region exhibits strong absorption because of leaf chlorophyll content, and reflection is due to mesophyll cells [6].

The LAI of crop is a key variable for estimating the foliage cover and photosynthetic processes, ultimately aids in forecasting of the crop growth and yield [7]. The estimation of LAI includes direct and indirect measurement methods. The direct measurement of LAI includes destructive sampling and laboratory evaluation which is time-consuming, labor-intensive, discontinuous and is not applicable for large-scale investigations [8,9]. Therefore, numerous research efforts have been emphasized on the indirect measurement of LAI using remote sensing technology due to its non-destructive and rapid monitoring potential [10,11].

Among various vegetation indices (VI) and neural network approaches, the scaled normalized difference vegetation index (NDVI) methodology was the most efficient way to retrieve LAI [12].

© 2023 by the author(s). Distributed under a Creative Commons CC BY license.

Preprints (www.preprints.org) | NOT PEER-REVIEWED | Posted: 26 December 2023 doi:10.20944/preprints202312.2021.v1

However, it is sensitive to atmospheric processes, soil conditions and saturates at low LAI [13]. Thus, other VIs *viz.,* modified red-edge normalized difference vegetation index (mND_{705}) [14], soil adjusted vegetation index (SAVI) [15], triangular vegetation index [16], and renormalized difference vegetation index (RDVI) [17] were developed to enhance the precision of LAI estimation. The VIs with red-edge bands are better predictors of LAI [18–21]. Recently, hyperspectral remote sensing has drawn the emphasis on LAI estimation because it provides continuous spectral coverage and achieves a spectral resolution of <10 nm in the range of 400-2500 nm [4,22]. Mapping the distribution of LAI in winter wheat for various growth phases was performed using UAV-based hyperspectral data [9] and AVIRIS-NG data [23]. Many studies in rice revealed that the VIs were positively correlated with biomass during pre-heading stages and negatively during post-heading stages [24,25].

To maximize the effectiveness of LAI estimation, identification of significant wave bands in the hyperspectral data is essential for retrieving more specific VIs [26]. Further, the combination of these wave bands under diverse environmental conditions and cultural practices provides appropriate information for the characterization of LAI with the crop phenological stages [27]. In this study, we examined the utility of different VIs through hyperspectral measurements from airborne AVIRIS-NG to map LAI at various phenological stages of rice.

2. Materials and Methods

2.1. Study Area

The study area is Banaganapalle mandal, Kurnool district, Andhra Pradesh, India in which rice is predominantly cultivated in both wet and dry seasons. The wet season plantings were carried out during July-August and dry season plantings during November-December. Rice is mostly transplanted and in few cases direct seeding was noticed in the study area. The soils are predominantly vertisols, and rice was grown following the recommended agronomic practices. Farmers mostly cultivate rice varieties *viz.,* BPT 5204, NDLR-7, RP Bio-226 and BPT 2270 of medium to long (130-160 days) crop growth duration.

2.2. Sampling Sites and Field Data Collection

Ground-truth surveying of rice fields was carried out during fourth week of February, 2018 (20-24 February) and the AVIRIS NG images were acquired on 26 February, 2018 which has spectral range of 380-2510 nm with spatial resolution of 4-8 m. Farmers' fields were surveyed based on the stratified random sampling procedure. A total of 132 fields in Banaganapalle were selected randomly during the dry season for rice LAI estimation at various phenological phases (15.723°N to 15.979°N latitude; 77.926°E to 78.186°E longitude) (Appendix A1, Figure 1). The dates of sowing and transplanting were recorded through farmer's interaction and rice growth stages observed at the time of data collection. The plantings varied considerably and lasted for three months from second week of November, 2017 to first week of February, 2018. The harvesting was done for a period of two months *i.e.,* from first week of March to second week of May, 2018. Field measurements of in-situ LAI was recorded from the surveyed fields individually during or near the AVIRIS-NG airborne data acquisition.

Preprints (www.preprints.org) | NOT PEER-REVIEWED | Posted: 26 December 2023 doi:10.20944/preprints202312.2021.v1

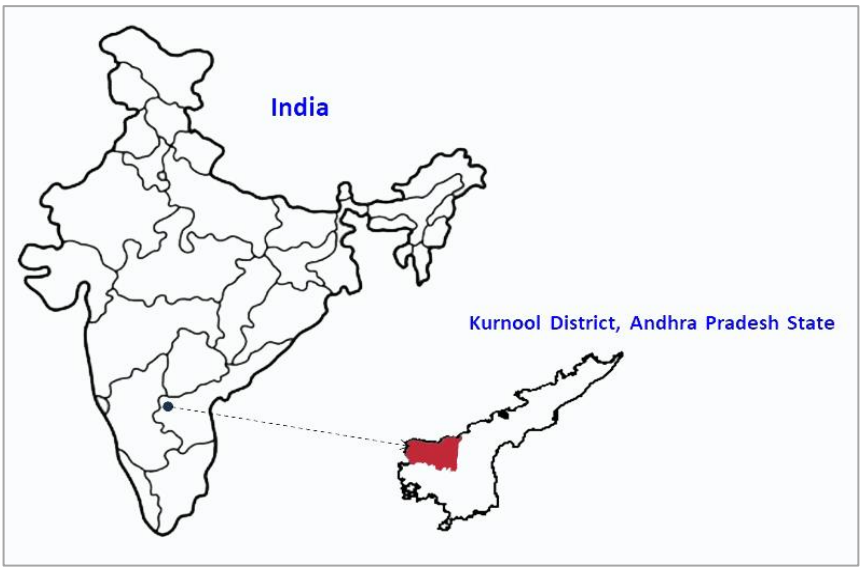

Appendix A1. Map of India representing the study area.

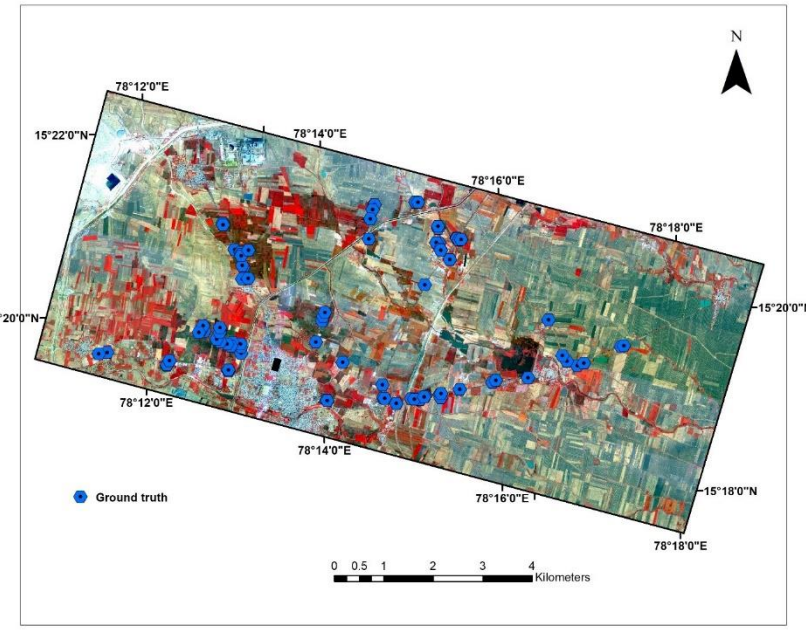

Figure 1. FCC of the study area and the sampling sites.

2.3. Sampling of LAI

Field surveys were conducted from 132 farmer's fields for ground-truth data collection (Figure 2). As the study area is a traditional rice growing belt, the crop was observed at different phenological stages. Accordingly, the fields were categorized into seven phenological stages (Table 1) as seedling (planted in first to second week of February), tillering (planted in fourth week of January), elongation (planted during second week of January), booting (planted in first week of January), heading (planted during fourth week of December), flowering (planted during second week of December), and maturity (planted during second week of November) (Figure 3). The surveyed fields were segregated separately for calibration (78 fields) and validation (54 fields) to estimate LAI using remote sensing (Table 1). Five plants were selected randomly from each surveyed field for non-destructive LAI measurement using SunScan plant canopy analyzer (Delta-T devices Ltd, UK) representing each phenological stage.

Preprints (www.preprints.org) | NOT PEER-REVIEWED | Posted: 26 December 2023 doi:10.20944/preprints202312.2021.v1

Table 1. Details of rice fields sampled at different phenological stages.

Crop growth stage	Field samples considered for calibration	Field samples considered for validation
Seedling	14	12
Tillering	19	12
Elongation	9	7
Booting	11	7
Heading	10	6
Flowering	8	5
Maturity	7	5
Total	**78**	**54**

Figure 2. Ground-truth data collection in the study area.

Figure 3. Rice crop at various growth phases (a) Seedling; (b) Tillering; (c) Elongation; (d) Heading; (e) Flowering; (f) Maturity.

2.4. Canopy Spectral Reflectance Measurements

Canopy spectral reflectance measurements from rice were recorded with FieldSpec 3 Hi-Res spectroradiometer (ASD Inc., USA; spectral range: 350-2500 nm). All the spectral measurements were made during 20-24 February, 2018 between 11:00 and 14:00 hr Indian standard time (GMT + 5.30 hrs) under clear sky. The radiometer was configured to record 30 scans for each sample, and 15-25 plants from each

Preprints (www.preprints.org) | NOT PEER-REVIEWED | Posted: 26 December 2023 doi:10.20944/preprints202312.2021.v1

field were sampled at the time of data recording. The pistol grip of radiometer was positioned at 1 m above the crop canopy, centered over the rice hills, with 25° FOV foreoptic to ensure the reflectance from a single desired plant. Prior to field measurements, the spectral radiometer was warmed-up for about 20 min to avoid the spectral steps at detector overlap wavelength regions, which occur due to different warm-up rates for the three spectroradiometer arrays [28]. The sampling interval was 1.4 nm at 350-1000 nm range, and 2 nm at 1000-2500 nm range. The spectral resolution (full width half maximum) was 3 nm at 700 nm, 6.5 nm at 1400 nm, and 8.5 nm at 2100 nm. Finally, the collected spectral data was exported to RS2 software and interpolated using ASD ViewSpecPro software in the post processing to produce values at each nanometer [29]. The spectral reflectance data from 1300-1400 nm and 1800-1950 nm were not considered for analysis due to noise caused by atmospheric water absorption in the raw spectrum.

2.5. AVIRIS-NG Airborne Data Acquisition

The present study is part of the collaborative program between Indian Space Research Organization (ISRO), India and Jet Propulsion Laboratory (JPL), NASA; Department of Science & Technology, Government of India and many other research organizations including the Indian Council of Agricultural Research (ICAR). AVIRIS-NG data covers a wavelength range of 380-2510 nm in VNIR and SWIR spectral channels, with a contiguous spectral band of 425 at a 5 nm interval. Spatially, it has a varying resolution of 4-8 m with a flying altitude of 4-8 km for a swath of 4-6 km. The AVIRIS-NG radiance data were orthorectified using input geometry files (IGM) present with the data containing the original line number and sample number for georeferencing and later atmospheric correction was carried out.

2.6. Data Processing

AVIRIS-NG data Endmember spectra was collected using ENVI software for the selected locations in farmers field. Correlation analysis was performed for spectral reflectance and LAI. Highly correlated spectral bands were used to calculate the new band ratios and estimate the relevant vegetation indices. The regression analysis was performed between vegetation indices and LAI. Descriptions and formulas of VIs used in the study are listed in Table 2.

Table 2. Hyperspectral vegetation indices used in the study.

Spectral Vegetation Index	Formula	Reference
VOG 1	$\left(\frac{R_{740}}{R_{720}}\right)$	[30]
MTCI	$(R_{850} - R_{730})/(R_{730} - R_{675})$	[31]
VOG 2	$(R_{734} - R_{747})/(R_{715} + R_{726})$	[30]
MSR	$\frac{\left((R_{800}/R_{670}) - 1\right)}{\left(\sqrt{(R_{800}/R_{670})} + 1\right)}$	[32]
mND_{705}	$\frac{(R_{750} - R_{705})}{(R_{750} + R_{705} - 2 * R_{445})}$	[33]
DD	$(R_{749} - R_{720}) - (R_{701} - R_{672})$	[34]
GNDVI	$(R_{750} - R_{550})/(R_{750} + R_{550})$	[35]
OSAVI	$(1 + 0.16)(R_{800} - R_{670})/(R_{800} + R_{670} + 0.16)$	[36]
RDVI	$\frac{R_{800} - R_{670}}{\sqrt{R_{800} + R_{670}}}$	[17]
SR	$\frac{R_{800}}{R_{670}}$	[37]

Preprints (www.preprints.org) | NOT PEER-REVIEWED | Posted: 26 December 2023 doi:10.20944/preprints202312.2021.v1

MTVI 2	$\frac{1.5 * 1.2 * (R_{800} - R_{550}) - 2.5 * (R_{670} - R_{550})}{\sqrt{(2 * R_{800} + 1)^2 - (6 * R_{800} - 5 * \sqrt{R_{670}}) - 0.5}}$	[13]
SAVI	$\left(\frac{R_{800} - R_{670}}{R_{800} + R_{670} + 0.5}\right)(1 + 0.5)$	[15]
NDVI	$(R_{810} - R_{680})/(R_{810} + R_{680})$	[38]
RVI	(R_{810}/R_{680})	[39]
EVI 1	$2.5 * (R_{860} - R_{645})/(1 + R_{860} + 6 * R_{645} - 7.5 * R_{470})$	[40]
DVI	$(R_{810} - R_{680})$	[39]
PRI	$(R_{570} - R_{531})/(R_{570} + R_{531})$	[41]
TVI	$\frac{120 * (R_{750} - R_{550}) - 200 * (R_{670} - R_{550})}{2}$	[16]
DDn	$2 * R_{710} - R_{660} - R_{760}$	[42]
MSR_{705}	$\frac{R_{750} - R_{445}}{R_{705} - R_{445}}$	[33]
MNLI	$\frac{(1 + 0.5) * (R_{810}^2 - R_{680})}{(R_{810}^2 + R_{680} + 0.5)}$	[43]
SIPI	$\frac{R_{800} - R_{445}}{R_{800} - R_{680}}$	[44]
WI	$\frac{R_{900}}{R_{970}}$	[45]
RVSI	$\frac{R_{714} - R_{752}}{2} - R_{733}$	[46]
Slaidi	$S * \frac{R_{1050} - R_{1250}}{R_{1050} + R_{1250}} * R_{1555}$ where S=5	[47]
NDWI	$(R_{858} - R_{2130})/(R_{858} + R_{2130})$	[48]
NDII	$\frac{R_{819} - R_{1600}}{R_{819} + R_{1600}}$	[49]
REP	$R_{700} + 40 * \left[\frac{(R_{670} + R_{780})}{2} - R_{700}\right]/(R_{740} - R_{700})$	[50]
WDRVI	$\frac{(0.2 * R_{800} - R_{670})}{(0.2 * R_{800} + R_{670})} + \frac{(1 - 0.2)}{(1 + 0.2)}$	[51]

2.7. Data Analysis

The mean reflectance values of LAI at different phenological stages was obtained from different rice fields (area ranged from 0.5 to 10.0 ha) to find out the sensitive wavebands for each phenological stage. The descriptive statistics of LAI and vegetation indices at different phenological stages were performed, and means along with standard deviation were presented. Coefficient of determination (R^2) and root mean square error (RMSE) were used to evaluate the prediction accuracy of the regression models [52], as they are the indicators of how well regression models (best-fit function) capture the relationship between LAI and vegetation indices. Regression analysis was performed between LAI and vegetation indices for

Preprints (www.preprints.org) | NOT PEER-REVIEWED | Posted: 26 December 2023 doi:10.20944/preprints202312.2021.v1

calibration and validation of the data and R^2 and RMSE were presented. Statistical analysis was performed using SAS Institute Inc. [53].

3. Results

3.1. Reflectance Spectra of Rice Canopy from Hand held Hyperspectral Radiometry

The ground based mean canopy reflectance spectra of rice at different phenological stages was recorded and presented in Figure 4a. It was found that the spectral reflectance of rice showed variation at various phenological stages in ultraviolet (350-400 nm), visible (400-750 nm) and NIR regions (750-1100 nm) with maximum reflectance in the NIR region. In UV region, the canopy reflectance was maximum at tillering followed by seedling stage and the lowest was observed during flowering and maturity. Within the visible region, green region (490-560 nm) had higher reflectance compared to violet-blue (400-425 nm) and red region (640-685 nm). The reflectance in visible region increased as the crop advanced from seedling to tillering and reduced from elongation to flowering, with the lowest reflectance at heading. The reflectance in the NIR region varied steadily with crop phenological stage, indicating a distinct variation in the spectral pattern that can be leveraged to identify the crop phenological stage.

3.2. Reflectance Spectra of Rice Canopy from AVIRIS-NG

The air borne spectral reflectance showed marked variation similar to ground-truth spectra at different phenological stages, as shown in Figure 4b. The variations in spectral reflectance were observed in UV, visible and NIR regions with increased reflectance in NIR region and reduced reflectance in both UV and visible regions. The findings of canopy reflectance observed in ground-truth spectra were similar and consistent with the air borne spectral reflectance at different phenological stages. In UV region, maximum and minimum reflectance was noticed in tillering and maturity stages, respectively. Within visible region, the reflectance variations were clearly observed in the green region compared to violet-blue and red region, with the highest reflectance in tillering and lowest in elongation stage. In NIR region, the reflectance pattern exhibited increased trend from seedling to booting and reduced trend from flowering to maturity stage. From these results, it is evident that various crop growth phases of rice can be differentiated using airborne hyperspectral reflectance spectra.

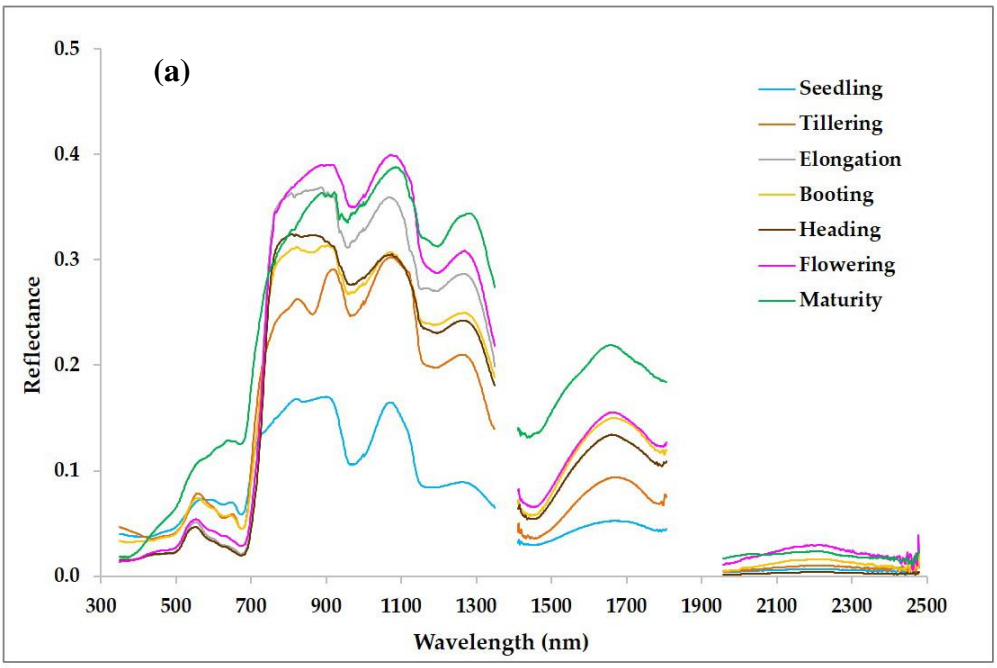

Preprints (www.preprints.org) | NOT PEER-REVIEWED | Posted: 26 December 2023 doi:10.20944/preprints202312.2021.v1

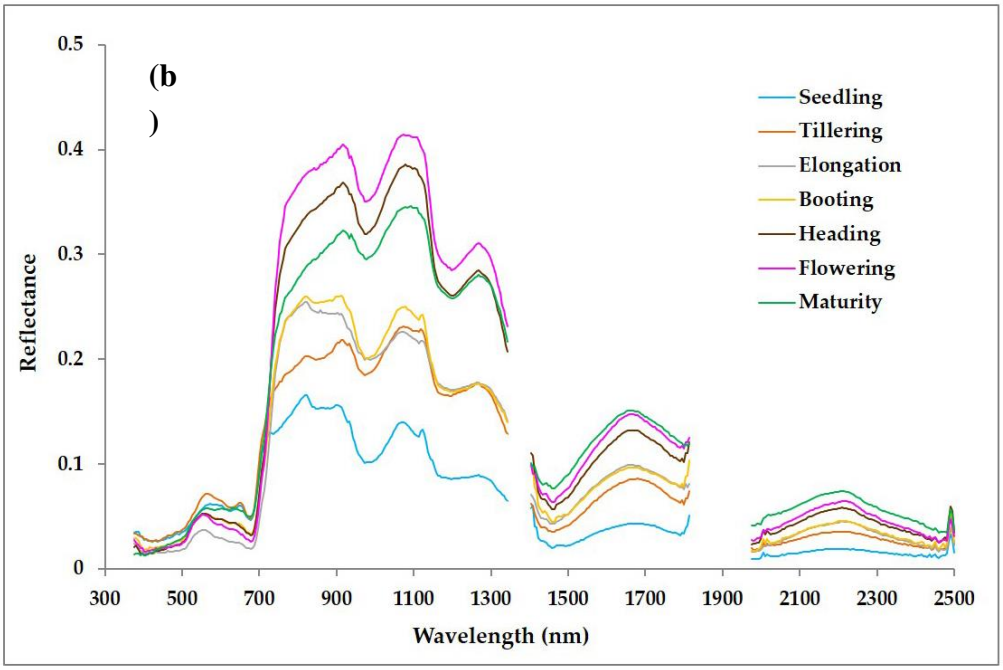

Figure 4. Hyperspectral signatures for different crop growth stages of rice recorded using (a) ground based measurements and (b) AVIRIS-NG.

3.3. Rice LAI at Different Phenological Stages

LAI measurements at different phenological stages were presented in Table 3. As the crop advances from seedling to maturity, variations in LAI were obvious with changing phenological stages. LAI increased from seedling to heading, and reached peak at flowering and reduced thereafter (1.21 at seedling to 3.61 at heading and flowering). The range of LAI was maximum at booting (1.70 to 4.00) followed by tillering (0.75 to 2.60) and elongation stage (1.60 to 3.00). The minimal variations in LAI were observed at maturity stage (1.60 to 2.50).

Table 3. Field measured Leaf Area Index (LAI) of rice at different crop growth stages used for model building.

Crop growth stage	Number of fields surveyed	LAI				
		Mean ± SD	Minimum	Maximum	P value	CV
Seedling	14	1.21 ± 0.45	0.54	2.20	0.59	37.50
Tillering	19	1.71 ± 0.54	0.75	2.60	0.68	31.66
Elongation	9	2.41 ± 0.53	1.60	3.00	0.12	21.79
Booting	11	3.00 ± 0.82	1.70	4.00	0.04	27.24
Heading	10	3.61 ± 0.47	3.10	4.30	0.15	13.00
Flowering	8	3.61 ± 0.45	2.80	4.10	0.42	12.49
Maturity	7	2.11 ± 0.35	1.60	2.50	0.38	16.48

3.4. Relationship of Vegetation Indices to Rice Phenological Stages

The vegetation indices used in the study showed marked variations with canopy growth from seedling to maturity stage. We used 29 vegetation indices to estimate rice LAI at varied phenological stages (Table 4). The relationship of different VIs with growth stages from seedling to heading were established. The temporal variations of these VIs increased from seedling to heading and later decreased till crop

Preprints (www.preprints.org) | NOT PEER-REVIEWED | Posted: 26 December 2023 doi:10.20944/preprints202312.2021.v1

maturity. Results showed that NDVI (0.54-0.91), SAVI (0.82-1.36), MSR (0.91- 3.54) and VOG (1.06-2.11) performed better. Similarly, other VIs *viz.,* WDRVI, OSAVI and GNDVI also performed better from seedling to heading with the values ranging between 0.50-1.27, 0.38-0.74 and 0.41-0.78, respectively. The SR (3.78-20.79), TVI (7.15-17.95) and RVI (3.83-21.75) showed relatively higher values, whereas MTVI 2 (0.17-0.47), mND_{705} (0.16-0.74) and RDVI (0.27-0.56) exhibited lower values from seedling to heading stage.

Table 4. Vegetation indices at different crop growth stages of rice estimated from AVIRIS-NG.

VI	Seedling	Tillering	Elongation	Booting	Heading	Flowering	Maturity
WI	1.80 ± 0.93	1.63 ± 0.69	1.24 ± 0.19	1.22 ± 0.18	1.18 ± 0.02	1.13 ± 0.03	1.07 ± 0.07
NDWI	0.26 ± 0.28	0.26 ± 0.20	0.14 ± 0.11	0.14 ± 0.08	0.15 ± 0.01	0.11 ± 0.03	0.04 ± 0.07
NDII	0.56 ± 0.20	0.54 ± 0.17	0.43 ± 0.11	0.44 ± 0.06	0.51 ± 0.01	0.46 ± 0.04	0.29 ± 0.14
SLAIDI	0.01 ± 0.00	0.01 ± 0.00	0.01 ± 0.00	0.01 ± 0.00	0.01 ± 0.00	0.01 ± 0.00	0.01 ± 0.00
NDVI	0.54 ± 0.14	0.64 ± 0.08	0.80 ± 0.08	0.82 ± 0.08	0.91 ± 0.02	0.84 ± 0.03	0.53 ± 0.21
OSAVI	0.38 ± 0.10	0.44 ± 0.07	0.58 ± 0.07	0.62 ± 0.08	0.74 ± 0.04	0.67 ± 0.04	0.43 ± 0.15
GNDVI	0.41 ± 0.09	0.49 ± 0.07	0.64 ± 0.08	0.67 ± 0.09	0.78 ± 0.02	0.71 ± 0.03	0.53 ± 0.11
RVSI	-0.01 ± 0.00	-0.01 ± 0.00	-0.01 ± 0.00	-0.01 ± 0.01	0.01 ± 0.00	-0.00 ± 0.00	-0.01 ± 0.00
REP	735.60 ± 64.56	728.59 ± 8.77	725.35 ± 1.64	725.43 ± 2.45	729.34 ± 0.54	727.22 ± 1.09	742.50 ± 16.60
SR	3.78 ± 1.43	4.89 ± 1.31	10.64 ± 4.44	12.01 ± 4.70	20.79 ± 3.97	11.82 ± 2.88	4.28 ± 2.68
RDVI	0.27 ± 0.07	0.31 ± 0.05	0.42 ± 0.06	0.45 ± 0.06	0.56 ± 0.04	0.50 ± 0.03	0.33 ± 0.11
SAVI	0.82 ± 0.21	0.97 ± 0.13	1.20 ± 0.12	1.23 ± 0.12	1.36 ± 0.03	1.26 ± 0.05	0.80 ± 0.32
MSR	0.91 ± 0.37	1.19 ± 0.30	2.19 ± 0.70	2.40 ± 0.70	3.54 ± 0.43	2.42 ± 0.41	0.98 ± 0.65
TVI	7.15 ± 2.86	8.00 ± 2.18	12.01 ± 2.47	13.69 ± 2.33	17.95 ± 2.07	15.94 ± 1.54	9.75 ± 4.18
MNLI	-0.41 ± 0.05	-0.40 ± 0.05	-0.47 ± 0.05	-0.50 ± 0.04	-0.60 ± 0.04	-0.57 ± 0.03	-0.51 ± 0.04
MTCI	0.58 ± 0.32	1.27 ± 0.49	2.80 ± 0.84	3.32 ± 1.33	6.26 ± 0.54	3.80 ± 0.83	1.69 ± 0.76
MTVI2	0.17 ± 0.06	0.20 ± 0.05	0.30 ± 0.06	0.34 ± 0.06	0.47 ± 0.06	0.40 ± 0.04	0.21 ± 0.11
PLS	1.40 ± 0.42	1.53 ± 0.33	2.07 ± 0.49	2.41 ± 0.38	3.26 ± 0.31	2.74 ± 0.37	1.99 ± 0.46
RVI	3.83 ± 1.49	4.84 ± 1.22	10.83 ± 4.54	12.71 ± 5.72	21.75 ± 3.91	11.95 ± 2.90	4.30 ± 2.73
DVI	0.14 ± 0.04	0.15 ± 0.03	0.22 ± 0.05	0.25 ± 0.04	0.35 ± 0.04	0.31 ± 0.03	0.21 ± 0.06
PRI	0.13 ± 0.03	0.09 ± 0.02	0.05 ± 0.03	0.04 ± 0.03	0.00 ± 0.01	0.04 ± 0.02	0.09 ± 0.02
WDRVI	0.50 ± 0.19	0.64 ± 0.14	0.98 ± 0.20	1.03 ± 0.20	1.27 ± 0.06	1.06 ± 0.10	0.51 ± 0.31
VOG1	1.06 ± 0.09	1.19 ± 0.12	1.53 ± 0.19	1.62 ± 0.25	2.11 ± 0.09	1.72 ± 0.15	1.26 ± 0.19
mND_{705}	0.16 ± 0.10	0.31 ± 0.10	0.52 ± 0.09	0.56 ± 0.11	0.74 ± 0.02	0.60 ± 0.07	0.29 ± 0.16
MSR_{705}	0.71 ± 0.09	0.74 ± 0.05	0.86 ± 0.05	0.86 ± 0.06	0.91 ± 0.01	0.88 ± 0.02	0.79 ± 0.10
SIPI	1.27 ± 0.21	1.13 ± 0.08	1.05 ± 0.03	1.04 ± 0.05	1.01 ± 0.01	1.04 ± 0.02	1.41 ± 0.30

Preprints (www.preprints.org) | NOT PEER-REVIEWED | Posted: 26 December 2023 doi:10.20944/preprints202312.2021.v1

DDN	-0.20 ± 0.04	-0.21 ± 0.05	-0.32 ± 0.07	-0.37 ± 0.07	-0.54 ± 0.06	-0.46 ± 0.05	-0.41 ± 0.02
DD	-0.05 ± 0.01	-0.01 ± 0.02	0.04 ± 0.03	0.06 ± 0.04	0.13 ± 0.02	0.08 ± 0.02	0.00 ± 0.04
VOG2	-0.02 ± 0.01	-0.04 ± 0.02	-0.11 ± 0.04	-0.13 ± 0.07	-0.28 ± 0.03	-0.16 ± 0.04	-0.05 ± 0.04

The values are Mean ± Standard deviation.

3.5. Evaluation of Vegetation Indices for Rice LAI Estimation

The LAI data collected using hand held canopy analyzer during ground truthing showed higher LAI till heading stage, which was also found true when compared with the LAI estimated using AVIRIS-NG. These vegetation indices were subjected to regression analysis to build models for estimating LAI at each phenological stage. The regression analysis (R^2 and RMSE) was performed between LAI and VIs. The indices that are statistically significant at each phenological stage were represented in Table 5. The results showed that vegetation indices had significant relationship with LAI till booting stage only. Thereafter, at heading and flowering stages, the relationship was non-significant. Among the VIs, at seedling stage, SR ($R^2 = 0.66^{**}$, RMSE = 0.28), MSR ($R^2 = 0.65^{***}$, RMSE = 0.28), RVI ($R^2 = 0.65^{***}$, RMSE = 0.28) and WDRVI ($R^2 = 0.64^{***}$, RMSE = 0.28) captured LAI better than the other VIs. However, SAVI ($R^2 = 0.60^{**}$, RMSE = 0.29) and NDVI ($R^2 = 0.59^{**}$, RMSE = 0.30) exhibited slightly lower significant relationship with LAI at the same phenological stage. At tillering, though VOG2 ($R^2 = 0.52^{**}$, RMSE = 0.38) and PRI ($R^2 = 0.47^{**}$, RMSE = 0.41) had strong positive relationship, it was not considered as the best fit, since no relationship with LAI was observed at later phenological stages. The mND_{705} had exhibited strong relationship with LAI with better values ($R^2 = 0.44^{**}$, RMSE = 0.42), followed by NDVI ($R^2 = 0.42^{**}$, RMSE = 0.42) and SAVI ($R^2 = 0.42^{**}$, RMSE = 0.42). The DD ($R^2 = 0.30^{**}$, RMSE = 0.46) and GNDVI ($R^2 = 0.32^{*}$, RMSE = 0.46) had weak relationship at all phenological stages.

Interestingly, REP ($R^2 = 0.74^{**}$, RMSE = 0.29) and MSR_{705} ($R^2 = 0.70^{**}$, RMSE = 0.31) had captured LAI better than other VIs during elongation stage, but failed for rest of the phenological stages. The best-fit models of LAI and VI for elongation stage were NDVI ($R^2 = 0.69^{**}$, RMSE = 0.31), SAVI ($R^2 = 0.69^{**}$, RMSE = 0.31), WDRVI ($R^2 = 0.68^{**}$, RMSE = 0.32) and MSR ($R^2 = 0.66^{**}$, RMSE = 0.33), while the least fit model was with mND_{705} ($R^2 = 0.57^{*}$, RMSE = 0.37). At booting stage, WDRVI ($R^2 = 0.67^{**}$, RMSE = 0.49), NDVI ($R^2 = 0.65^{**}$, RMSE = 0.52), SAVI ($R^2 = 0.65^{**}$, RMSE = 0.51) and MSR ($R^2 = 0.64^{**}$, RMSE = 0.52) had strong relationship between LAI and VI whereas, RVI ($R^2 = 0.53^{*}$, RMSE = 0.59) had weak relationship at booting stage. Some of the other VIs *viz.*, RVSI, OSAVI, RDVI, MTVI2, TVI, mND_{705} and PLS were good at seedling stage; SIPI, VOG, MTCI and DD at tillering; SIPI, PRI, VOG and MTCI at elongation stage; SIPI, MSR_{705}, OSAVI, RDVI, MTVI2 and DD at booting stage (Table 5). The indices that had varied responses with different phenological stages was not considered for further validation.

Preprints (www.preprints.org) | NOT PEER-REVIEWED | Posted: 26 December 2023 doi:10.20944/preprints202312.2021.v1

Table 5. Best fit models for estimating LAI using different Vegetation Indices (VI) at different crop growth stages of rice.

VI	Seedling		VI	Tillering		VI	Elongation		VI	Booting		VI	Heading		VI	Flowering	
	R^2	RMSE		R^2	RMSE		R^2	RMSE		R^2	RMSE		R^2	RMSE		R^2	RMSE
SR	0.66***	0.28	VOG2	0.52***	0.38	REP	0.74**	0.29	WDRVI	0.67**	0.49	NDII	0.10^{ns}	0.47	PRI	0.44^{ns}	0.37
MSR	0.65***	0.28	PRI	0.47**	0.41	MSR_{705}	0.70**	0.31	NDVI	0.65**	0.52	WI	0.08^{ns}	0.48	REP	0.36^{ns}	0.39
RVI	0.65***	0.28	mND_{705}	0.44**	0.42	NDVI	0.69**	0.31	SAVI	0.65**	0.51	SIPI	0.08^{ns}	0.48	mND_{705}	0.36^{ns}	0.39
WDRVI	0.64***	0.28	NDVI	0.42**	0.42	SAVI	0.69**	0.31	MSR	0.64**	0.52	MSR_{705}	0.07^{ns}	0.48	SIPI	0.35^{ns}	0.39
SAVI	0.60**	0.29	SAVI	0.42**	0.42	WDRVI	0.68**	0.32	SIPI	0.62**	0.53	RVSI	0.05^{ns}	0.48	MTCI	0.33^{ns}	0.40
NDVI	0.59**	0.30	WDRVI	0.42**	0.42	MSR	0.66**	0.33	MSR_{705}	0.60**	0.55	REP	0.03^{ns}	0.49	VOG2	0.32^{ns}	0.40
RVSI	0.59**	0.30	MSR	0.41**	0.42	SR	0.65**	0.33	SR	0.59**	0.55	SR	0.02^{ns}	0.49	RVSI	0.26^{ns}	0.42
OSAVI	0.57**	0.31	RVI	0.41**	0.43	SIPI	0.64*	0.34	mND_{705}	0.59**	0.55	MSR	0.01^{ns}	0.50	VOG	0.25^{ns}	0.42
RDVI	0.56**	0.31	SIPI	0.41**	0.43	RVI	0.60*	0.36	OSAVI	0.58**	0.56	TVI	0.01^{ns}	0.50	NDVI	0.24^{ns}	0.42
GNDVI	0.55**	0.32	SR	0.40**	0.43	GNDVI	0.58*	0.37	GNDVI	0.54*	0.58	MNLI	0.01^{ns}	0.50	SR	0.24^{ns}	0.42
MTVI2	0.55**	0.32	VOG	0.40**	0.43	mND_{705}	0.57*	0.37	RDVI	0.54*	0.58	PLS	0.01^{ns}	0.50	SAVI	0.24^{ns}	0.42
TVI	0.53**	0.32	MTCI	0.38**	0.44	PRI	0.55*	0.38	MTVI2	0.53*	0.59	RVI	0.01^{ns}	0.49	MSR	0.24^{ns}	0.42
mND_{705}	0.52**	0.32	GNDVI	0.32*	0.46	VOG	0.54*	0.38	RVI	0.53*	0.59	DVI	0.01^{ns}	0.50	WDRVI	0.24^{ns}	0.42
PLS	0.48**	0.34	DD	0.30*	0.46	MTCI	0.51*	0.39	DD	0.52*	0.60	mND_{705}	0.01^{ns}	0.50	DD	0.24^{ns}	0.43

* Significant at 0.05% | ** Significant at 0.01% | *** Significant at 0.001% | ns: non-significant.

Preprints (www.preprints.org) | NOT PEER-REVIEWED | Posted: 26 December 2023 doi:10.20944/preprints202312.2021.v1

3.6. Validation of VIs for Estimation of LAI

The best fit VIs were validated using independent data sets of 54 field locations. As the crop growth advanced from seedling to flowering, the LAI increased. Thereafter, it decreased till maturity stage. The maximum deviations in LAI were noticed in the booting stage ranging from 2.50-4.10. The minimal variations were observed in the seedling stage *i.e.,* from 0.60-1.31 (Table 6, Figure 5). Further, the R^2 and RMSE of the validation dataset at four phenological stages were calculated for all the best-fit models, but only the significant ones are represented in Table 7. Among several VIs that were found statistically significant, only 8 VIs were identified to estimate LAI at all the phenological stages except booting stage. For booting stage, only 2 VIs were found significant. The R^2 and RMSE values differed for each phenological stage and vegetation indices. Similar to the calibration data, VIs showed differential response at each stage with fluctuating R^2 values and the best prediction was observed at elongation stage.

Table 6. Field measured LAI of rice at different crop growth stages used for validation of models.

Crop growth stage	Number of fields	LAI				
		Mean ± SD	Minimum	Maximum	P value	CV (%)
Seedling	12	0.99 ± 0.23	0.60	1.31	0.33	23.51
Tillering	12	1.78 ± 0.40	1.20	2.42	0.42	22.41
Elongation	7	2.89 ± 0.40	2.50	3.60	0.29	13.80
Booting	7	3.29 ± 0.58	2.50	4.10	0.88	17.70
Heading	6	3.63 ± 0.35	3.20	4.20	0.92	9.64
Flowering	5	3.79 ± 0.57	2.90	4.50	0.42	15.11
Maturity	5	2.24 ± 0.68	1.50	3.10	0.53	30.38

Preprints (www.preprints.org) | NOT PEER-REVIEWED | Posted: 26 December 2023 doi:10.20944/preprints202312.2021.v1

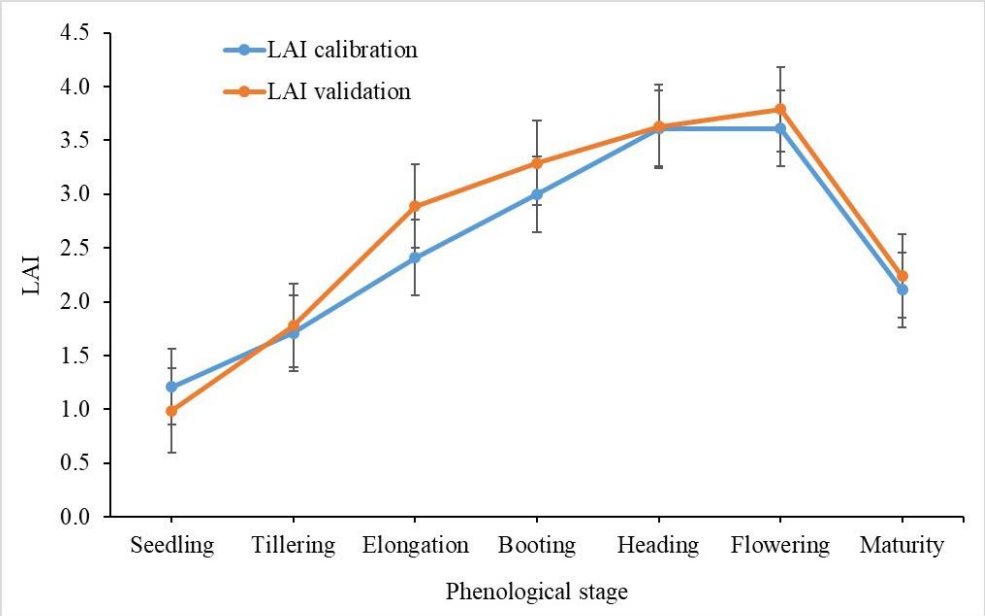

Figure 5. LAI of rice fields used for calibration and validation of data.

Table 7. Estimated LAI at different crop growth stages of rice (Validation of model outputs).

VI	Seedling		Tillering		Elongation		Booting	
	R^2	RMSE	R^2	RMSE	R^2	RMSE	R^2	RMSE
mND_{705}	0.52**	0.17	0.42*	0.32	0.88**	0.15	0.51^{ns}	0.45
SR	0.50**	0.17	0.40*	0.32	0.66*	0.26	0.10^{ns}	0.60
MSR	0.51**	0.17	0.48*	0.30	0.67*	0.25	0.42^{ns}	0.49
RVI	0.51**	0.17	0.38*	0.33	0.71*	0.24	0.10^{ns}	0.60
WDRVI	0.47*	0.18	0.37*	0.33	0.76*	0.22	0.62*	0.39
SAVI	0.49*	0.17	0.56**	0.28	0.63*	0.27	0.59*	0.41
NDVI	0.45*	0.18	0.34*	0.34	0.73*	0.23	0.54^{ns}	0.43
GNDVI	0.49*	0.17	0.45*	0.31	0.83**	0.18	0.50^{ns}	0.45

* Significant at 0.05% | ** Significant at 0.01% | ns: non-significant.

At seedling stage, strong correlation between LAI and mND_{705} ($R^2 = 0.52^{**}$) was observed that indicated the best fit model followed by MSR and RVI ($R^2 = 0.51^{**}$). Other VIs *viz.*, SR, WDRVI, SAVI, NDVI and GNDVI have significant correlation and have R^2 values ranging from 0.45 to 0.50. At tillering stage, SAVI ($R^2 = 0.56^{**}$) followed by MSR ($R^2 = 0.48^{*}$) proved best fit with field LAI. Other VIs which are statistically significant include GNDVI ($R^2 = 0.45^{*}$), mND_{705} ($R^2 = 0.42^{*}$), SR ($R^2 = 0.40^{*}$), WDRVI ($R^2 = 0.37^{*}$), RVI ($R^2 = 0.38^{*}$) and NDVI ($R^2 = 0.34^{*}$). The best estimation of LAI was noticed at elongation stage ($R^2 = 0.63$- 0.88). The best fit model with strong correlation was noticed between LAI and mND_{705} which had maximum R^2 (0.88^{**}) followed by GNDVI (0.83^{**}). The performance of VIs *viz.*, WDRVI, NDVI and RVI were better ($R^2 = > 0.70^{*}$) compared to MSR, SR and SAVI ($R^2 = <0.70^{*}$) at elongation stage. At booting stage, only two VIs *viz.*, WDRVI (0.62^{*}) and SAVI (0.59^{*}) found strongly correlated with LAI and rest of the VIs were non-significant. The satellite images of the best-performing VIs for LAI estimation of the selected fields *viz.*, mND_{705}, SAVI and WDRVI were depicted in Figure 6 respectively.

Our results showed that RMSE values also differed with phenological stages. The lower RMSE values were observed at seedling (0.17-0.18) and elongation stages (0.15-0.27) compared to tillering

Preprints (www.preprints.org) | NOT PEER-REVIEWED | Posted: 26 December 2023 doi:10.20944/preprints202312.2021.v1

(0.28-0.34) and booting (0.39-0.60). The models with least RMSE value will predict better. Thus, seedling stage can be estimated better followed by elongation stage. The estimation of LAI with VIs at booting stage was not significantly correlated when compared to other three phenological stages. Hence, most of the indices performed better at later phenological stages (elongation stage, the canopy was fully exposed) compared to early stages (seedling and tillering).

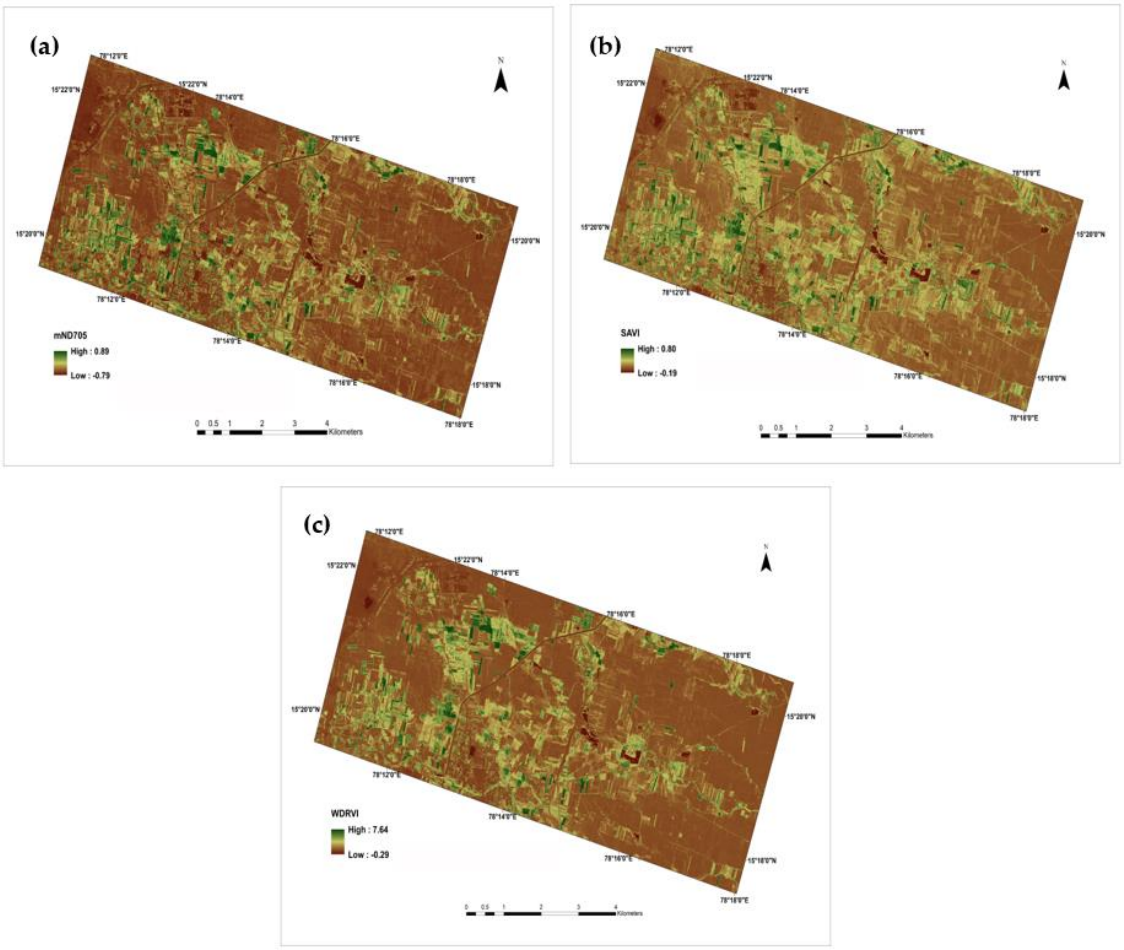

Figure 6. Estimated Leaf Area Index (LAI) of rice fields with (a) mND705; (b) SAVI; (c) WDRVI.

4. Discussion

This study aims to estimate the rice LAI at different phenological stages *viz.*, seedling, tillering, elongation, booting, heading, flowering and maturity using AVIRIS-NG hyperspectral data and ground measured LAI data. The results indicated that the relationship of LAI with vegetation indices at different phenological stages was distinct (Table 5). Rice plant undergoes distinct changes in the canopy at different phenological stages during the growing season. As the rice plants grow from seedling to booting, the growth flourishes. Once the plant enters the reproductive stage (heading stage), the panicles start emerging, bringing changes in the canopy architecture. Our findings revealed that LAI increased upto heading and thereafter decreased (Table 3). The similar changes in LAI at different growth phases of rice has been reported earlier [54,55].

The reflectance data of both ground-based hyperspectral radiometry and AVIRIS-NG showed marked variations between phenological stages and identical trend was noticed in both the ground based and airborne hyperspectral data (Figure 4). The results further sowed that the spectral reflectance increased and reached peak value at booting and reduced thereafter at ripening phase. The canopy reflectance is governed by biophysical characteristics of vegetation, architecture of the canopy, atmospheric absorption, and scattering, direction of incidence radiation and soil

Preprints (www.preprints.org) | NOT PEER-REVIEWED | Posted: 26 December 2023 doi:10.20944/preprints202312.2021.v1

backgrounds [56]. As higher photosynthetic activity takes place during vegetative stage of rice, the plants absorb more photosynthetically active radiation from the visible region [57], and variations in the reflectance in visible region was low during this stage when compared to heading stage, where the panicles start emerging on the top of canopy (Figure 4b). Contrarily, in NIR region, the canopy reflectance of rice from ripening stages (heading to maturity) tend to be higher compared to vegetative stages (Figure 4b). During early vegetative stage of rice, the canopy reflectance was reduced due to slow growth and increased exposure to soil and water. As the crop advances to reproductive stage, the growth hastens and increased reflectance was noticed from elongation to flowering, probably due to increased leaf area and reduced exposure of soil [58,59]. Spectral reflectance in the visible region is mainly influenced by pigment absorption, while the reflectance in NIR region is determined by canopy structure and the changes in leaf orientation from horizontal to vertical at critical stages owing to overlapping of leaves, chlorotic and necrotic turning during senescence [60–63].

The vegetation indices tested in this study were calculated based on the ratio or difference between NIR and visible reflectance, having distinct response at different phenological stages. These vegetation indices have been used in the past for estimating biophysical parameters *viz.*, LAI, chlorophyll and biomass in several crops [24,64,65]. Our findings revealed that there was significant correlation between LAI and VIs at different phenological stages (Table 5) and these results are in accordance with previous studies [66,67]. The ground measured LAI was best fitted with the VIs at elongation stage (R^2 = 0.51-0.74, $p<0.05$) and tillering (R^2 = 0.30-0.52, $p<0.05$) followed by booting stage (R^2 = 0.52 to 0.67, $p<0.05$), suggesting that rice LAI can be predicted better at elongation stage. This shows that the 51-74% variability in vegetation indices could be explained by LAI, while the remaining 26-49% variation could probably attribute to different agronomic management practices *viz.*, crop variety, fertilizer management, planting time etc. Validation of LAI with vegetation indices at different phenological stages showed that the performance was low at seedling (R^2 = 0.45-0.52), tillering (R^2 = 0.34-0.56) and booting (R^2 = 0.10-0.62), whereas better performance was observed at elongation stage (R^2 = 0.63-0.88). The LAI of rice crop at vegetative stages was upto 3.0 and indices *viz.*, mND_{705}, SR, MSR, RVI, WDRVI, SAVI, NDVI and GNDVI better predicted LAI across all the stages from seedling to booting with few exceptions (Table 7). Whereas, from heading to maturity, there was no relationship between LAI and VIs.

The best performing VIs for LAI have bands at green, red, blue and NIR regions. These findings agreed with the earlier reports by Thenkabail et al. [67], Darvishzadeh et al. [68] and Herrmann et al. [69] suggesting that the red-edge and NIR bands are important for LAI assessment and possess strong influence to strengthen the relationship between spectral reflectance and LAI. At seedling and elongation stages, the mND_{705} accurately predicted the LAI which consists of the combination of red-edge, blue and NIR bands suggesting that blue bands can also have influence in LAI estimation [70–72]. This index effectively reduces the impact of differences in leaf surface reflectance and improves the sensitivity of pigment content estimation [33]. At tillering stage, SAVI with red and NIR bands predicted LAI better and similar reports were observed by He et al. [73]. This could be because, in contrast to the NDVI, SAVI increases the linearity between the index and LAI and normalizes the soil-induced changes from spectral vegetation indices without affecting the vegetation measures [15]. At booting stage, WDRVI with red and NIR bands predicted better LAI with strong relationship and explained 62% of variation in LAI. This might be due to the higher sensitivity of WDRVI to moderate-to-high LAI (between 2 and 6) that aid in monitoring the vegetation status and precision farming [74]. Earlier studies also established the WDRVI vegetation index for accurate estimation of LAI in maize, soybean, wheat and potato [75,76]. The distinct variation of VIs for LAI at different phenological stages was likely due to the leaf angle within the canopy rather than individual leaf reflectance properties [65,77].

5. Conclusions

In this study, eight hyperspectral vegetation indices were found promising for estimating rice LAI at different phenological stages. Among all the stages, LAI at elongation stage was the best

Preprints (www.preprints.org) | NOT PEER-REVIEWED | Posted: 26 December 2023 doi:10.20944/preprints202312.2021.v1

predicted using AVIRIS-NG airborne hyperspectral sensors. The findings revealed different vegetation indices for different phenological stages. Red-edge, Blue and NIR bands were found sensitive for seedling and elongation stages, whereas, Red and NIR bands for tillering and booting stages. The results revealed that the best suitable hyperspectral vegetation indices for mapping and estimating LAI in rice were mND_{705} at seedling and elongation stages, SAVI at tillering and WDRVI at booting stage. The feasibility of using AVIRIS NG airborne hyperspectral sensors with very high spatial resolution for precise mapping of LAI from rice crop is demonstrated in the present study.

Author Contributions: Conceptualization, M.P.; methodology, K.A.G. and U.S.S.; software, G.S.S.; validation, M.T.; formal analysis, M.T., U.S.S. and G.S.K.; investigation, M.P., K.A.G. and N.R.K.; resources, M.P.; data curation, M.T., U.S.S., G.S.K. and P.C.; writing – original draft preparation, U.S.S. and P.C.; writing – review and editing, M.P., K.A.G. and N.R.K.; visualization, M.P.; supervision, M.P.; project administration, V.K.S.; funding acquisition, M.P. All authors have read and agreed to the published version of the manuscript.

Funding: This work was funded by Department of Science and Technology, Government of India, Network project Big Data Analytics – Hyperspectral Data (BDA-HSRS), Grant Number BDID/01/23/2014-HSRS18.

Acknowledgments: We gratefully acknowledge the farmers for their cooperation during field surveys and collecting ground-truth data. We thankfully acknowledge the support of staff and facilities under the Indian Council of Agricultural Research (ICAR) - National Innovations in Climate Resilient Agriculture (NICRA) project in analyzing the field samples and statistical analysis.

Conflicts of Interest: The authors declare no conflicts of interest.

References

1. World Rice Production 2022/2023. Available online: http://www.worldagriculturalproduction.com/crops/rice.aspx/ (accessed on 21 September 2022).
2. Thenkabail, P.S.; Smith, R.B.; Pauw, E.D. Hyperspectral vegetation indices and their relationship with agricultural crop characteristics. *Remote Sens. Environ.* **2000,** *71,* 152-182.
3. Atzberger, C.; Darvishzadeh, R.; Immitzer, M.; Schlerf, M.; Skidmore, A.; Le Maire, G. Comparative analysis of different retrieval methods for mapping grassland leaf area index using airborne imaging spectroscopy. *Int. J. Appl. Earth Obs. Geoinf.* **2015,** *43*, 19-31.
4. Prabhakar, M.; Gopinath, K.A.; Kumar, N.R.; Thirupathi, M.; Sravan, U.S.; Kumar, G.S.; Siva, G.S.; Meghalakshmi, G.; Vennila, S. Detecting the invasive fall armyworm pest incidence in farm fields of southern India using Sentinel-2A satellite data. *Geocarto Int.* **2021,** *37*, 3801-3816.
5. Lillesand, T.; Kiefer, R.W.; Chipman, J. *Remote Sensing and Image Interpretation*, 7th ed.; John Wiley & Sons: New Jersey, United States, **2015.**
6. Datt, B. Remote sensing of Chlorophyll a, Chlorophyll b, Chlorophyll a+b, and total Carotenoid content in Eucalyptus leaves. *Remote Sens. Environ.* **1998,** *66*, 111-121.
7. Chen, J.M.; Black, T. Defining leaf area index for non-flat leaves. *Plant, Cell Environ.* **1992,** *15*, 421-429.
8. Jonckheere, I.; Fleck, S.; Nackaerts, K.; Muys, B.; Coppin, P.; Weiss, M.; Baret, F. Review of methods for *in-situ* leaf area index determination: Part, I. Theories, sensors and hemispherical photography. *Agric. For. Meteorol.* **2004,** *121,* 19-35.
9. Tao, H.; Feng, H.; Xu, L.; Miao, M.; Long, H.; Yue, J.; Li, Z.; Yang, G.; Yang, X.; Fan, L. Estimation of crop growth parameters using UAV-based hyperspectral remote sensing data. *Sensors* **2020,** *20,* 1296.
10. Chen, Y.; Zhang, Z.; Tao, F. Improving regional winter wheat yield estimation through assimilation of phenology and leaf area index from remote sensing data. *Eur. J. Agron.* **2018,** *101,* 163-173.
11. Srinet, R.; Nandy, S.; Patel, N. Estimating leaf area index and light extinction coefficient using Random Forest regression algorithm in a tropical moist deciduous forest, India. *Ecol. Inform.* **2019,** *52,* 94-102.
12. Walthall, C.; Dulaney, W.; Anderson, M.; Norman, J.; Fang, H.; Liang, S. A comparison of empirical and neural network approaches for estimating corn and soybean leaf area index from Landsat ETM+ imagery. *Remote Sens. Environ.* **2004**, *92*, 465–474.
13. Haboudane, D.; Miller, J.R.; Pattey, E.; Zarco-Tejada, P.J.; Strachan, I.B. Hyperspectral vegetation indices and novel algorithms for predicting green LAI of crop canopies: Modeling and validation in the context of precision agriculture. *Remote Sens. Environ.* **2004**, *90*, 337–352.
14. He, L.; Ren, X.; Wang, Y.; Liu, B.; Zhang, H.; Liu, W.; Feng, W.; Guo, T. Comparing methods for estimating leaf area index by multi-angular remote sensing in winter wheat. *Sci. Rep.* **2020,** *10*, 13943.
15. Huete, A.R. A soil-adjusted vegetation index (SAVI). *Remote Sens. Environ.* **1988,** *25*, 295–309.

Preprints (www.preprints.org) | NOT PEER-REVIEWED | Posted: 26 December 2023 doi:10.20944/preprints202312.2021.v1

16. Broge, N.H.; Leblanc, E. Comparing prediction power and stability of broadband and hyperspectral vegetation indices for estimation of green leaf area index and canopy chlorophyll density. *Remote Sens. Environ.* **2001**, *76*, 156–172.
17. Roujean, J.; Breon, F. Estimating PAR absorbed by vegetation from bidirectional reflectance measurements. *Remote Sens. Environ.* **1995**, *51*, 375–384.
18. Ma, B.L.; Dwyer, L.M.; Costa, C.; Cober, E.R.; Morrison, M.J. Early prediction of soybean yield from canopy reflectance measurements. *Agron. J.* **2001,** *93,* 1227–1234.
19. Clevers, J.; de Jong, S.M.; Epema, G.F.; van der Meer, F.D.; Bakker, W.H.; Skidmore, A.K.; Scholte, K.H. Derivation of the red edge index using the MERIS standard band setting. *Int. J. Remote Sens.* **2002**, *23*, 3169–3184.
20. Vina, A.; Gitelson, A.A.; Nguy-Robertson, A.L.; Peng, Y. Comparison of different vegetation indices for the remote assessment of green leaf area index of crops. *Remote Sens. Environ.* **2011**, *115*, 3468–3478.
21. Berger, K.; Atzberger, C.; Danner, M.; D'Urso, G.; Mauser, W.; Vuolo, F.; Hank, T. Evaluation of the PROSAIL model capabilities for future hyperspectral model environments: A review study. *Remote Sens.* **2018,** *10*, 85.
22. Jensen, J.R. *Remote Sensing of the Environment: An Earth Resource Perspective*, 2nd ed.; Pearson Education India: Noida, Uttar Pradesh, India, 2009.
23. Singh, P.; Srivastava, P.K.; Mall, R.K.; Bhattacharya, B.K.; Prasad, R. A hyperspectral R based leaf area index estimator: Model development and implementation using AVIRIS-NG. *Geocarto Int.* **2022,** *37*, 12792-12809.
24. Wang, Y.; Zhang, K.; Tang, C.; Cao, Q.; Tian, Y.; Zhu, Y.; Cao, W.; Liu, X. Estimation of rice growth parameters based on linear mixed-effect model using multispectral images from fixed-wing unmanned aerial vehicles. *Remote Sens.* **2019,** *11*, 1371.
25. Zheng, H.; Cheng, T.; Zhou, M.; Li, D.; Yao, X.; Tian, Y.; Cao, W.; Zhu, Y. Improved estimation of rice aboveground biomass combining textural and spectral analysis of UAV imagery. *Precis. Agric.* **2019,** *20*, 611-629.
26. Ryu, C.; Suguri, M.; Umeda, M. Model for predicting the nitrogen content of rice at panicle initiation stage using data from airborne hyperspectral remote sensing. *Biosyst. Eng.* **2009,** *104*, 465-475.
27. Nakanishi, T.; Imai, Y.; Morita, T.; Akamatsu, Y.; Odagawa, S.; Takeda, T.; Kashimura, O. Evaluation of wheat growth monitoring methods based on hyperspectral data of later grain filling and heading stages in Western Australia. *Int. Arch. Photogramm. Remote Sens. Spat. Inf. Sci.* **2012,** *39*, 295-300.
28. Delalieux, S.; Auwerkerken, A.; Verstraeten, W.W.; Somers, B.; Valcke, R.; Lhermitte, S.; Keulemans, J.; Coppin, P. Hyperspectral reflectance and fluorescence imaging to detect scab induced stress in apple leaves. *Remote Sens.* **2009,** *1*, 858-874.
29. ASD. *Technical Guide*. 4th ed. Boulder (CO): Analytical Spectral Devices Inc.; 1999; p. 136.
30. Vogelmann, J.E.; Rock, B.N.; Moss, D.M. Red-edge spectral measurements from Sugar Maple leaves. *Int. J. Remote Sens.* **1993,** *14*, 1563–1575.
31. Dash, J.; Curran, P.J. The MERIS terrestrial chlorophyll index. *Int. J. Remote Sens.* **2004,** *25*, 5403–5413.
32. Chen, J.M. Evaluation of vegetation indices and a modified simple ratio for boreal applications. *Can. J. Remote. Sens.* **1996,** *22*, 229–242.
33. Sims, D.A.; Gamon, J.A. Relationships between leaf pigment content and spectral reflectance across a wide range of species, leaf structures and developmental stages. *Remote Sens. Environ.* **2002,** *81*, 331–354.
34. LeMaire, G.; François, C.; Dufrene, E. Towards universal broad leaf chlorophyll indices using PROSPECT simulated database and hyperspectral reflectance measurements. *Remote Sens. Environ.* **2004,** *89*, 1–28.
35. Gitelson, A.A.; Merzlyak, M.N. Remote estimation of chlorophyll content in higher plant leaves. *Remote Sens.* **1997,** *18*, 2691–2697.
36. Rondeaux, G.; Steven, M.; Baret, F. Optimization of soil-adjusted vegetation indices. *Remote Sens. Environ.* **1996,** *55*, 95–107.
37. Birth, G.S.; McVey, G. Measuring the color of growing turf with a reflectance spectrophotometer. *Agron. J.* **1968,** *60*, 640-643.
38. Rouse, J.W.; Haas, R.H.; Schell, J.A.; Deering, D.W.; Harlan, J.C. Monitoring the vernal advancements and retrogradation of natural vegetation. In NASA/GSFC, Final Report, Greenbelt, MD, USA, 1974; pp. 1–137.
39. Jordan, C.F. Derivation of leaf area index from quality of light on the forest floor. *Ecology* **1969,** *50*, 663–666.
40. Huete, A.; Didan, K.; Miura, T.; Rodriguez, E.P.; Gao, X.; Ferreira, L.G. Overview of the radiometric and biophysical performance of the MODIS vegetation indices. *Remote Sens. Environ.* **2002,** *83*, 195-213.
41. Gamon, J.A.; Penuelas, J.; Field, C.B. A narrow-waveband spectral index that tracks diurnal changes in photosynthetic efficiency. *Remote Sens. Environ.* **1992,** *41*, 35–44.
42. Le Maire, G., Francois, C., Soudani, K., Berveiller, D., Pontailler, J.Y., Breda, N., Genet, H., Davi, H.; Dufrene, E. Calibration and validation of hyperspectral indices for the estimation of broadleaved forest leaf

Preprints (www.preprints.org) | NOT PEER-REVIEWED | Posted: 26 December 2023 doi:10.20944/preprints202312.2021.v1

chlorophyll content, leaf mass per area, leaf area index and leaf canopy biomass. *Remote Sens. Environ.* **2008,** *112*, 3846-3864.

43. Gong, P.; Pu, R.; Biging, G.S.; Larrieu, M.R. Estimation of forest leaf area index using vegetation indices derived from Hyperion hyperspectral data. IEEE Trans. Geosci. Remote Sens. **2003,** *41*, 1355-1362.
44. Penuelas, J.; Filella, I. Reflectance assessment of mite effects on apple trees. *Int. J. Remote Sens.* **1995,** *16*, 2727–2733.
45. Penuelas, J.; Pinol, J.; Ogaya, R.; Lilella, I. Estimation of plant water content by the reflectance water index WI (R900/R970). *Int. J. Remote Sens.* **1997,** *18*, 2869–2875.
46. Merton, R.; Huntington, J. Early simulation results of the ARIES-1 satellite sensor for multi-temporal vegetation research derived from AVIRIS. In Proceedings of the eighth annual JPL airborne earth science workshop, Pasadena, CA, USA, February 1999; pp. 9-11.
47. Delalieux, S.; Somers, B.; Hereijgers, S.; Verstraeten, W.W.; Keulemans, W.; Coppin, P. A near-infrared narrow-waveband ratio to determine Leaf Area Index in orchards. *Remote Sens. Environ.* **2008,** *112*, 3762-3772.
48. Gu, Y.; Brown, J.F.; Verdin, J.P.; Wardlow, B. A five-year analysis of MODIS NDVI and NDWI for grassland drought assessment over the central Great Plains of the United States. *Geophys. Res. Lett.* **2007,** *34*, L06407.
49. Hardisky, M.A.; Klemas, V.; Smart, R.M. The influence of soil salinity, growth form, and leaf moisture on the spectral radiance of *Spartina alterniflora* canopies. *Photogram. Eng. Remote Sens.* **1983,** *49*, 77–83.
50. Guyot, G.; Guyon, D.; Riom, J. Factors affecting the spectral response of forest canopies: A review. *Geocarto Int.* **1988,** *4*, 3-18.
51. Peng, Y.; Gitelson, A.A.; Keydan, G.; Rundquist, D.C.; Moses, W. Remote estimation of gross primary production in maize and support for a new paradigm based on total crop chlorophyll content. *Remote Sens. Environ.* **2011,** *115*, 978-989.
52. Govaerts, Y.M.; Verstraete, M.M.; Pinty, B.; Gobron, N. Designing optimal spectral indices: A feasibility and proof of concept study. *Int. J. Remote Sens.* **1999,** *20*, 1853-1873.
53. SAS Institute Inc. SAS OnlineDocVR 9.2. Cary (NC): 2009 [accessed on 20 June 2023]. http://support.sas.com/documentation.
54. Liu, Z.; Huang, W.; Mao, G.; Li, C.; Xu, X.; Ding, X.; Shi, J.; Zhou, B. Estimating foliar pigment concentration of rice crop using integrated hyperspectral index. In *Computer and Computing Technologies in Agriculture V: CCTA 2011.* IFIP Advances in Information and Communication Technology. Beijing, China, October 29-31; D. Li, Y. Chen Eds. Springer: Berlin, Heidelberg, Germany, 2011, 264-274.
55. Wu, L.; Yuan, S.; Huang, L.; Sun, F.; Zhu, G.; Li, G.; Fahad, S.; Peng, S.; Wang, F. Physiological mechanisms underlying the high-grain yield and high-nitrogen use efficiency of elite rice varieties under a low rate of nitrogen application in China. *Front. Plant Sci.* **2016,** *7*, 1024.
56. Carvalho, S.; Van der Putten, W.H.; Hol, W.H.G. The potential of hyperspectral patterns of winter wheat to detect changes in soil microbial community composition. *Front. Plant Sci.* **2016,** *7*, 759.
57. Lima, I.P.; Jorge, R.G.; de Lima, J.L.M.P. Remote sensing monitoring of rice fields: Towards assessing water saving irrigation management practices. *Front. Remote Sens.* **2021**, *2*, 762093.
58. Din, M.; Zheng, W.; Rashid, M.; Wang, S.; Shi, Z. Evaluating hyperspectral vegetation indices for leaf area index estimation of *Oryza sativa* L. at diverse phenological stages. *Front. Plant Sci.* **2017,** *8*, 820.
59. Kawamura, K.; Ikeura, H.; Phongchanmaixay, S.; Khanthavong, P. Canopy hyperspectral sensing of paddy fields at the booting stage and PLS regression can assess grain yield. *Remote Sens.* **2018,** *10*, 1249.
60. Gausman, H.W.; Allen, W.A.; Cardenas, R. Reflectance of cotton leaves and their structure. *Remote Sens. Environ.* **1969,** *1*, 19–22.
61. Woolley, J.T. Reflectance and transmittance of light by leaves. *Plant Physiol.* **1970,** *47*, 656–662.
62. Feng, W.; Guo, B.B.; Wang, Z.J.; He, L.; Song, X.; Wang, Y.H.; Guo, T.C. Measuring leaf nitrogen concentration in winter wheat using double-peak spectral reflection remote sensing data. *Field Crop Res.* **2014**, *159*, 43–52.
63. Gaju, O.; Allard, V.; Martre, P.; Le Gouis, J.; Moreau, D.; Bogard, M.; Hubbart, S.; Foulkes, M.J. Nitrogen partitioning and remobilization in relation to leaf senescence, grain yield and grain nitrogen concentration in wheat cultivars. *Field Crop Res.* **2014,** *155*, 213–223.
64. Peng, Y.; Nguy-Robertson, A.; Arkebauer, T.; Gitelson, A.A. Assessment of canopy chlorophyll content retrieval in maize and soybean: Implications of hysteresis on the development of generic algorithms. *Remote Sens.* **2017,** *9*, 226.
65. Dong, T.; Liu, J.; Shang, J.; Qian, B.; Ma, B.; Kovacs, J.M.; Walters, D.; Jiao, X.; Geng, X.; Shi, Y. Assessment of red-edge vegetation indices for crop leaf area index estimation. *Remote Sens. Environ.* **2019,** *222*, 133-143.

Preprints (www.preprints.org) | NOT PEER-REVIEWED | Posted: 26 December 2023 doi:10.20944/preprints202312.2021.v1

66. Chen, J. Gu, S. Shen, M. Tang, Y. Matsushita, B. Estimating aboveground biomass of grassland having a high canopy cover: An exploratory analysis of *in-situ* hyperspectral data. *Int. J. Remote Sens.* **2009,** *30,* 6497-6517.
67. Thenkabail, P.S.; Lyon, J.G.; Huete, A. *Biophysical and biochemical characterization and plant species studies,* 2nd ed.; CRC Press: Florida, United States, 2018.
68. Darvishzadeh, R.; Atzberger, C.; Skidmore, A.K.; Abkar, A.A. Leaf Area Index derivation from hyperspectral vegetation indices and the red edge position. *Int. J. Remote Sens.* **2009,** *30,* 6199–6218.
69. Herrmann, I. Pimstein, A. Karnieli, A. Cohen, Y. Alchanatis, V. Bonfil, D.J. LAI assessment of wheat and potato crops by VENμS and Sentimel-2 bands. *Remote Sens Environ.* **2011,** *115,* 2141-2151.
70. Li, F.; Miao, Y.; Hennig, S.D.; Gnyp, M.L.; Chen, X.; Jia, L.; Bareth, G. Evaluating hyperspectral vegetation indices for estimating nitrogen concentration of winter wheat at different growth stages. *Precis. Agric.* **2010,** *11,* 335–357.
71. Motohka, T.; Nasahara, K.N.; Oguma, H.; Tsuchida, S. Applicability of green-red vegetation index for remote sensing of vegetation phenology. *Remote Sens.* **2010,** *2,* 2369–2387.
72. Inoue, Y.; Sakaiya, E.; Zhu, Y.; Takahashi, W. Diagnostic mapping of canopy nitrogen content in rice based on hyperspectral measurements. *Remote Sens. Environ.* **2012,** *126,* 210–221.
73. He, J.; Zhang, N.; Su, X.; Lu, J.; Yao, X.; Cheng, T.; Zhu, Y.; Cao, W.; Tian, Y. Estimating leaf area index with a new vegetation index considering the influence of rice panicles. *Remote Sens.* **2019,** *11,* 1809.
74. Gitelson, A.A. Wide dynamic range vegetation index for remote quantification of biophysical characteristics of vegetation. *J. Plant Physiol.* **2004,** *161,* 165-173.
75. Nguy-Robertson, A.L.; Peng, Y.; Gitelson, A.A.; Arkebauer, T.J.; Pimstein, A.; Herrmann, I.; Karnieli, A.; Rundquist, D.C.; Bonfil, D.J. Estimating green LAI in four crops: Potential of determining optimal spectral bands for a universal algorithm. *Agric. For. Meteorol.* **2014,** *192,* 140–148.
76. Kira, O.; Nguy-Robertson, A.L.; Arkebauer, T.J.; Linker, R.; Gitelson, A.A. Toward generic models for green LAI estimation in maize and soybean: Satellite observations. *Remote Sens.* **2017,** *9,* 318.
77. Kattenborn, T.; Fassnacht, F.E.; Schmidtlein, S. Differentiating plant functional types using reflectance: Which traits make the difference? *Remote. Sens. Ecol. Conserv.* **2019,** *5,* 5-19.

Disclaimer/Publisher's Note: The statements, opinions and data contained in all publications are solely those of the individual author(s) and contributor(s) and not of MDPI and/or the editor(s). MDPI and/or the editor(s) disclaim responsibility for any injury to people or property resulting from any ideas, methods, instructions or products referred to in the content.